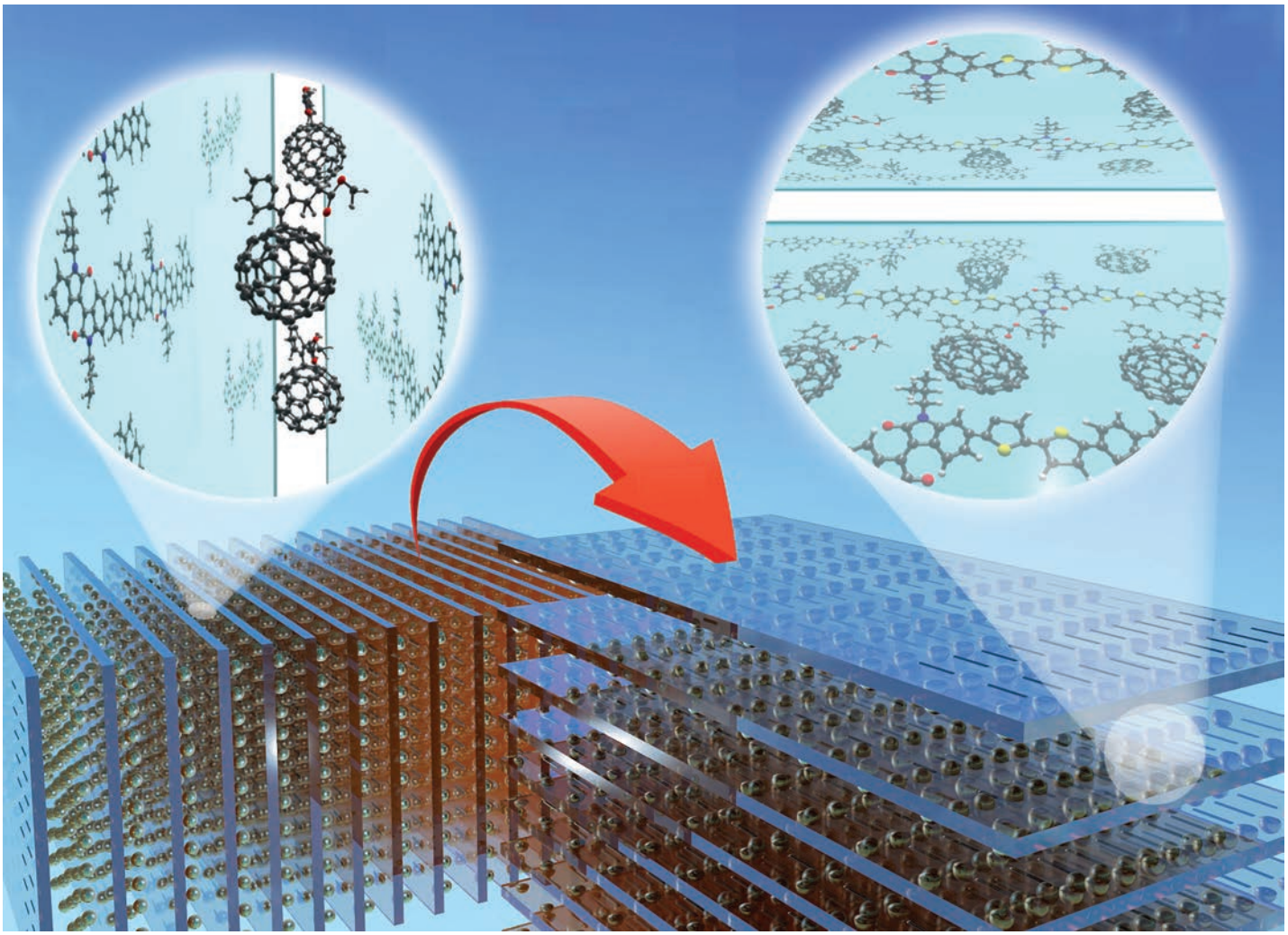

Showcasing research from the Nano and Information Materials Lab at Konkuk University, Seoul, Republic of Korea.

Akylidenefluorene-Isoindigo Copolymers with an Optimized Molecular Conformation for Spacer Manipulation, π-π Stacking and Its Application in Efficient Photovoltaic Devices

Performance of the varied length of thiophene spacers in copolymers, giving crystallinity differences based on the tilt angle. The long thiophene spacer makes $PC_{70}BM$ penetrate tightly between the polymer chains and enhances J_{SC} and PCE.

As featured in:

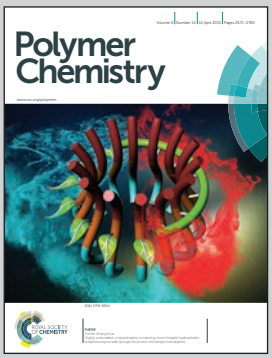

See Doo Kyung Moon *et al.* *Polym. Chem.*, 2015, **6**, 2636.

ROYAL SOCIETY OF CHEMISTRY

www.rsc.org/polymers

Registered charity number: 207890

Polymer Chemistry

PAPER

View Article Online
View Journal | View Issue

Cite this: *Polym. Chem.*, 2015, **6**, 2636

Alkylidenefluorene–isoindigo copolymers with an optimized molecular conformation for spacer manipulation, π–π stacking and their application in efficient photovoltaic devices†

Min-Hee Choi, Kwan Wook Song and Doo Kyung Moon*

Received 2nd January 2015,
Accepted 23rd February 2015

DOI: 10.1039/c5py00003c

www.rsc.org/polymers

D–$(\pi)_n$-A-type copolymers with different thienyl spacers (n = 0–2) between alkylidenefluorene and isoindigo (P1, P2, P3) were synthesized *via* a Suzuki coupling reaction. As the number of spacers was increased in a polymer (P1), the UV-Vis absorption maximum (λ_{max}) red-shifted, and the band gap decreased from 1.83 to 1.64 eV. The highest occupied molecular orbital (HOMO) levels of the polymers were increased by increasing the number of spacers. In addition, the facile intermixing due to better accessibility with the PCBM led to an increase in the hole mobility and J_{SC}. In contrast to P1 and P2, when the P3 thin films were blended with $PC_{70}BM$ in the X-ray diffraction (XRD) measurement, an increased face-on structure of the crystal was observed. The power conversion efficiency (PCE) of P3 was 3.0% and it reached 4.2% for the inverted device fabricated at 1 : 2 ratio with $PC_{70}BM$.

1. Introduction

Polymer solar cells (PSCs) have received considerable attention in academic research and industrial application in recent years due to their inexpensive manufacturing. In particular, the bulk heterojunction (BHJ) system, which employs a conjugated polymer (as the electron donor) and fullerene (as the electron acceptor) blend, has been widely studied. For PSCs, enhanced molecular engineering technology with π-conjugated polymers has recently emerged as a major research area. To enhance the power conversion efficiency (PCE) of the PSCs, the optoelectronic properties of the π-conjugated polymer, which is a photoactive material, should be tuned. An ideal conjugated polymer for PSCs should satisfy the following conditions: a low bandgap to enlarge the absorption region in the visible and near-infrared regions, high absorption coefficient, high hole mobility, a suitable highest occupied molecular orbital (HOMO)–lowest unoccupied molecular orbital (LUMO) level, and excellent miscibility with fullerene.[1,2] The PCE of the PSCs was enhanced to more than 7–9% by identifying the relationship between the chemical structure of the polymer and its photovoltaic performance.[3–6] To verify the state-of-the-art device performance of the polymer, research focused on controlling the crystallinity of the polymer in the solid-state at the nanoscale is required.[7–9]

Alberto Salleo *et al.* reported that increased solid-state packing *via* strong π–π stacking leads to high crystallinity.[10] In addition, I. McCulloch *et al.* proposed polyalkylidenefluorenes for application in solution-processable organic semiconductors, which have a high charge carrier mobility and environmental stability. Alkylidenefluorene is an electron-rich unit that has a rigid planar structure, and this unit increases the π–π stacking of the resulting polymer, imparts high mobility, decreases the HOMO level, and facilitates efficient conjugation from the chain length direction.[11] The alkylidenefluorene homopolymer has a significantly small intermolecular distance (<0.4 nm) that facilitates a coplanar conformation.[12]

In a previous study, we reported that the energy level and steric hindrance of the polymer could be adjusted according to the location of the side chain in the D–π-A type polymer.[8] The results indicated that the polymer without side chains from the spacer and acceptor exhibited the lowest band gap due to aggregation caused by strong π-stacking and possessed a low solubility and molecular weight. However, when the side chain was implemented in the spacer, the lowest PCE was observed due to the steric hindrance and edge-on rich structure. Most semiconducting organic materials exhibit anisotropic charge transport properties, where the electric charge effectively moves from the π-stacking direction.[13,14]

Department of Materials Chemistry and Engineering, Konkuk University, 1 Hwayang-dong, Gwangjin-gu, Seoul 143-701, Korea. E-mail: dkmoon@konkuk.ac.kr; Fax: +82-2-444-0765; Tel: +82-2-450-3498

† Electronic supplementary information (ESI) available: Synthetic procedures for preparation of monomers and polymers, characterization data, ^{1}H-NMR spectra of polymers, *J–V* characteristics of the hole-only devices based on polymer : $PC_{70}BM$ blends, morphologies of the polymer : PCBM blend films and additional OPV characteristics at different D : A ratios. See DOI: 10.1039/c5py00003c

In a D–A-type polymer, Mikkel Jørgensen *et al.* adjusted the length of the spacer of the polymer with alkoxyphenylbenzothiadiazole.[15] David G. Lidzey *et al.* published research results based on adjusting the length of the spacer of the anthracene-benzothiadiazole polymer. As the number of spacers increased, the band gap decreased, and the differences in J_{SC} and PCE were insignificant. UV-Vis absorption spectra were red-shifted when the numbers of spacers were increased. Recently, Tajima *et al.* reported dithienopyrrole–benzothiadiazole copolymers with some different opto-electric results when a spacer was introduced. Their polymers showed blue-shifted spectra.[16]

In contrast, the solubility and energy levels of isoindigo, which allow for implementation of various side chains with two –N groups through lactam rings, can be easily tuned. Furthermore, isoindigo has been successfully introduced in the field of organic electronics to form donor–acceptor (D–A) small molecules and polymers *via* a strong electron-deficient unit.[17–20] Isoindigo consisted of planar moieties that can form strong π–π stacks in the solid state. The hole and electron mobilities of isoindigo-based D–A conjugated polymers are 0.81 and 0.66 $cm^2\ V^{-1}\ s^{-1}$, respectively.[21] However, the results of X-ray crystal analysis of isoindigo confirmed the disadvantageous generation of a steric interaction in which a twist occurs near the central C=C bond between two indolinones.[22] Although the implementation of one thiophene between D–A units is known to enhance properties, limited studies have reported the implementation of bithiophene, which has primarily resulted in insoluble polymers.

In this study, alkylidenefluorene–isoindigo copolymers were synthesized using the Suzuki coupling reaction and these copolymers exhibit good solubility even when several thiophenes were employed. Thiophene and bithiophene were applied as π-bridges between the isoindigo and the alkylidenefluorene donor moiety. The structure–property relationship was observed for the length of the spacer. The results confirmed that the increased number of spacers decreased the twist angle between the donor and the acceptor, which led to an enhancement in the planarity, crystallinity, and PCBM intercalation. By applying the polymer with the bithiophene spacers, as an active layer, J_{SC} and FF increased and PCE was increased to 4.2%.

2. Results and discussion

2.1 Polymer synthesis

Scheme 1 shows typical synthetic routes to the monomers and polymers, as shown in Fig. 1. 9-(1′-Decylundecylidene)fluorene (D1) was used as a donor and 6,6′-dibromo-*N*,*N*′-(2-octyldodecyl)isoindigo (A0), which is a well-known organic dye, was used as an acceptor. In addition, thiophene and bithiophene were applied as conjugated linkers for the indigo derivatives in A0 to synthesize A1 and A2, respectively, as shown in Scheme 1. Poly[2,7-bis-9-(1-decylundecylidene)fluorene-*alt*-*N*,*N*′-(2-octyldodecyl)-6,6′-π-isoindigo] (P1, P2, P3) were synthesized using a Suzuki coupling reaction with D1 and indigo derivatives (A0–A2) (Fig. 1). Polymerization was performed at 90 °C for 48 h with $Pd(PPh_3)_4$(0), a 2 M aqueous potassium carbonate solution, Aliquat 336 as a surfactant, and toluene–THF or DMF = 1 : 1 as a solvent. After the polymerization was complete, end-capping was performed using bromobenzene and phenylboronic acid. The obtained powders were collected after being re-precipitated in methanol. Purification was performed sequentially with methanol, acetone, and chloroform using Soxhlet apparatus. Finally, the chloroform-soluble portion was re-precipitated in methanol. The obtained powders were reddish black (P1), blue-black (P2), and greenish black (P3) solids, and their yields were 76, 67, and 27%, respectively.

P1 and P2 were soluble in tetrahydrofuran (THF), chlorobenzene, and *o*-dichlorobenzene, and P3 was soluble only at an elevated temperature. The structure of the synthesized polymer was determined using ^{1}H-NMR spectroscopy (see Fig. S1 in ESI†). Isoindigo and the monomer of isoindigo with thiophene and bithiophene spacers were successfully synthesized, which was confirmed using the ^{1}H-NMR spectra. For the structure of the obtained polymers, the peak corresponding to P2 was determined to be between 7.08 and 6.8 ppm and 6.7–6.5 ppm due to the hydrogen atoms combined with the 3,4-carbon of the aromatic thiophene spacer. The peak corresponding to P3 was observed between 7.08 and 6.8 ppm and 6.7–6.5 ppm, which is the same peak observed for P2, due to the hydrogen atoms combined with the 3,4-carbon of the bithiophene spacer, and two additional hydrogen atoms were found compared with the number of hydrogen atoms found in P2. In addition, the NMR spectra exhibited a decreased resolution and increasingly broadened peaks in the order of P1 to P3. This phenomenon is typically observed in polymers that have several carbon types, due to overlapping of all of the chemical shift anisotropy lines, which leads to a broad spectrum.

Table 1 lists the results of the measurements of molecular weights of the polymers. As shown in Table 1, P1, P2, and P3 have average molecular weights (M_n) of 21.4, 28.2, and 19.3 kDa, respectively, and broad PDI of 2.50, 2.66, and 3.80, respectively. In comparison with P1 and P3, P2 exhibited a high degree of polymerization due to the application of an appropriate thiophene linker. The planarity of P1, which does not have the spacer, decreased due to a large tilted angle between the donor and phenyl rings of the acceptor resulting in increased steric hindrance, which led to a low degree of polymerization. Z. Peng *et al.* reported that when the distance of the phenyl and phenyl groups is close to the backbone of the polymers, the steric hindrance between the two groups increases, which makes it difficult to achieve a higher molecular weight.[23] Therefore, studies focused on effectively increasing the conjugation of the polymer main chain by improving the planarity between the donor and the acceptor through the application of a spacer (*e.g.*, P2 and P3) have been conducted. Jizheng Wang and David G. Lidzey *et al.* confirmed that the enhanced planarity between the donor and the acceptor through the implementation of a spacer leads to a broad

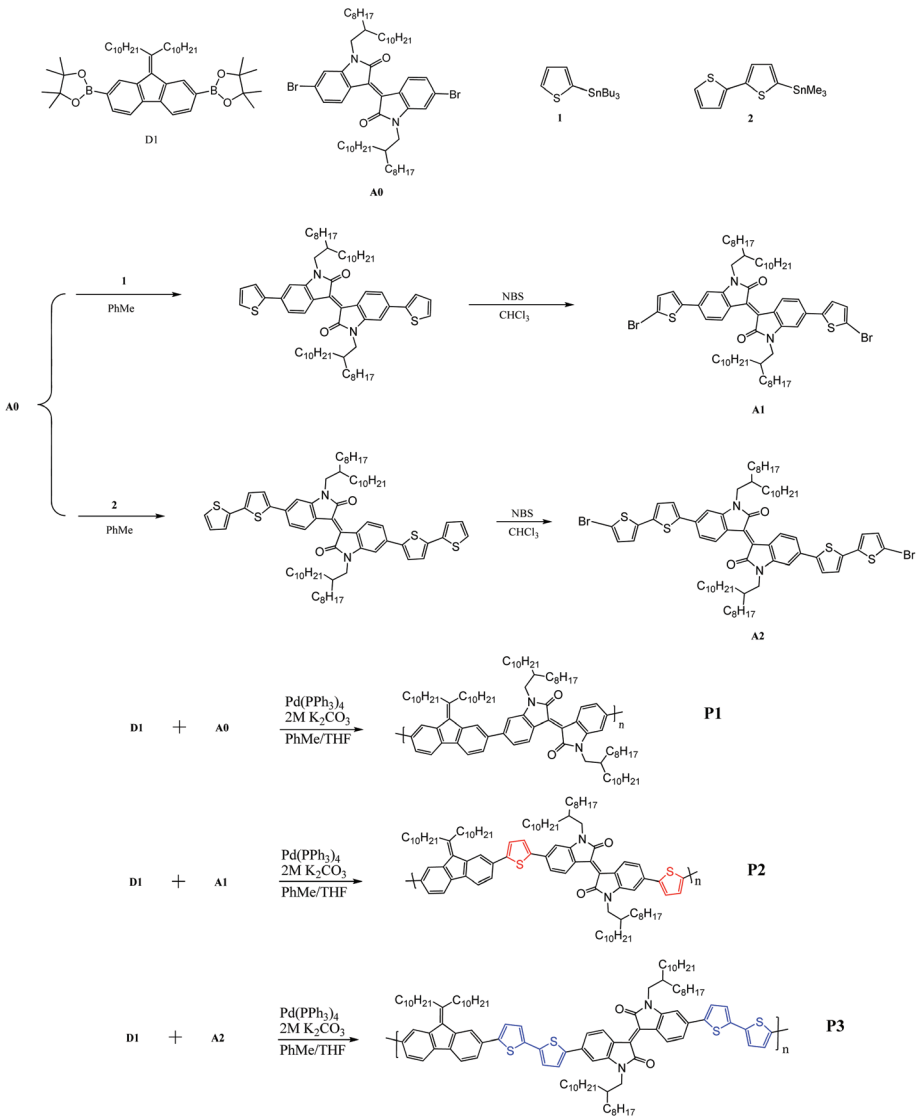

Scheme 1 Synthetic route to polymers.

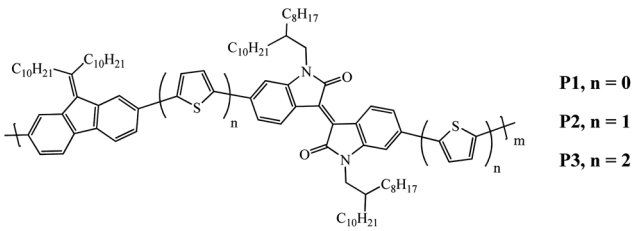

Fig. 1 Isoindigo based conjugated polymers with alkylidenefluorene donating units.

absorption range for the polymers and an excellent photovoltaic performance through the increased hole mobility.[24,25] However, for P3, the small side-chain moieties within the repeating unit after the implementation of a double thiophene linker reduced the solubility of the polymers, which resulted in precipitation during the polymerization, leading to a low degree of polymerization.

2.2 Optical and electrochemical properties

Fig. 2 shows the UV-visible spectra for the solution and film phases of the three polymers. All of the polymers were measured after being dissolved in chloroform at a concentration of 10 μg ml^{-1}. The results are summarized in Table 2. The maximum absorption peak (λ_{max}) of P1 was at 321 mm in the solution, and the absorption coefficient at this time was calculated to be 3.0×10^4 M^{-1} cm^{-1}. In the film, the peak (λ_{max} = 330 nm) was red-shifted by 9 mm compared to that in the solution. This red shift indicates that P1 has a strong π-stacking tendency due to aggregation of the polymer in the solid state. The absorption edge of P1 was at 678 nm, and the optical band gap calculated according to this edge was 1.83 eV,

Table 1 Physical and thermal properties of polymers

Polymer	Yield [%]	M_n [a] [kDa]	M_w [a] [kDa]	PDI[a]	Degree of polymerization[a]
P1	76	21.4	53.5	2.50	16
P2	67	28.2	75.0	2.66	19
P3	27	19.3	69.5	3.80	12

[a] Determined by GPC in tetrahydrofuran (THF) using polystyrene standards.

which is the largest value among those for the synthesized polymers in this study. Therefore, when the spacer is absent from the main chain, the polymer has the largest bandgap as well as a correspondingly narrow absorption area. The maximum absorption peak (λ_{max}) of P2 was at 615 nm in the solution, and its absorption coefficient was calculated to be 4.0×10^4 M^{-1} cm^{-1}. In the film phase, the peak (λ_{max} = 604 nm) was blue-shifted by 11 nm compared to that in the solution. The absorption edge of P2 was at 725 nm, and the optical band gap that was calculated according to this edge was 1.71 eV. In addition, in comparison with P1, the absorption spectra of P2 were red-shifted by 60 nm in the solution and by 35 nm in the film.

This confirms that P2 has a broader absorption area and a reduced band gap compared to P1 because the thiophene spacer was implemented between the alkylidenefluorene donor unit and the isoindigo acceptor unit. This decrease in the band gap is due to the effective increase in the conjugation length of the polymers.[26] The UV-visible spectra of P3 are similar to those of P2. A maximum absorption peak (λ_{max}) of P3 was determined at 622 nm in the solution, and its absorption coefficient was calculated to be 5.7×10^4 M^{-1} cm^{-1}. This value is greater than those for the P1 and P2 polymers, indicating that P3 facilitates greater optical absorption. The peak (λ_{max} = 617 nm) of P3 in the film phase was blue-shifted by 5 nm compared to that in the solution. The absorption edge of P3 was at 756 nm, and the optical band gap that was calculated according to this edge was 1.64 eV. This band gap value is the lowest among those for the synthesized polymers in this study.

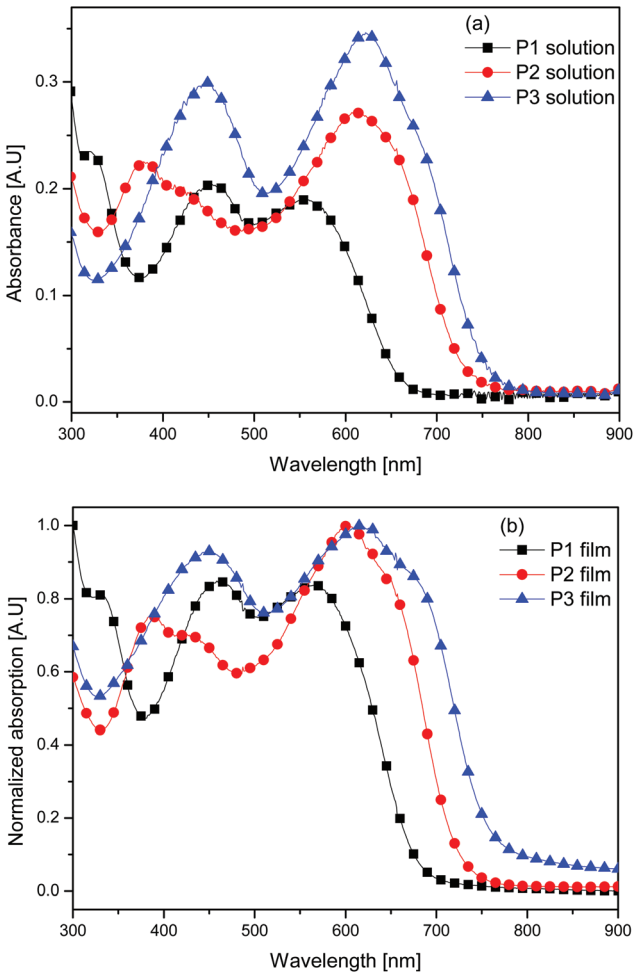

Fig. 2 UV-Vis absorption spectra of polymers in solution (a) and film (b).

These results are consistent with the research results reported by David G. Lidzey.[25] By comparing the spectra of P2 and P3, the optical absorption of P3 was red-shifted in the long-wavelength region in both the solution and film. Because a longer π spacer was applied using bithiophene, the main chain of the polymer forms a more planar conformation and has an extended electronic delocalization leading to an

Table 2 Optical and electrochemical data of polymers

	UV-Vis absorption						Cyclic voltammetry			
	$CHCl_3$ solution		Film							
Polymer	λ_{max} [nm]	λ_{sh} [nm]	λ_{max} [nm]	λ_{sh} [nm]	λ_{onset} [nm]	E_g^{op} [a] [eV]	E_{onset}^{ox} [V]	E_{onset}^{red} [V]	HOMO[b] [eV]	LUMO[c] [eV]
P1	321	453, 555	330	463, 569	678	1.83	1.52	−0.38	−5.89	−4.37
P2	615	376	604	389	725	1.71	1.35	−0.37	−5.72	−4.01
P3	622	447	617	447	756	1.64	1.23	−0.36	−5.60	−3.96

[a] Calculated from the intersection of the tangent on the low energetic edge of the absorption spectrum with the baseline. [b] $E_{HOMO} = -[E_{onset}(vs.\ Ag/AgCl) - E_{1/2}(Fc/Fc^+\ vs.\ Ag/AgCl)] - 4.8$ eV. [c] LUMO = HOMO + E_g.

increased conjugation length. The typical UV-visible spectra of the DA-type polymer primarily exhibit two absorption peaks. The peak in the high-energy area (300–500 nm) is caused by the π–π* transition of the donor segments (alkylidenefluorene derivatives)[27] and the peak in the low-energy area (500–800 nm) is caused by the intramolecular charge transfer (ICT) transition (isoindigo units) between the donor and the acceptor.[28] The optical absorption spectra for P2 and P3 showed the form mentioned above, and the optical absorption spectra for P1 showed two optical absorption peaks in the range of 300–500 nm. Therefore, P1 exhibited a total of three peaks. The second absorption peak for P1, which was observed at 453 nm in the solution and at 463 nm in the film, is generated by the n–π* transition due to aggregation of the expanded conjugation system through the C–N–C bonds of the alkylidenefluorene unit.[29] For P2 and P3, the effects of the expanded conjugation due to the spacer are greater than those due to the aggregation of the donor unit. Therefore, the n–π* transition is not observed due to a strong π–π* transition band. Because the UV spectrum of P1 was red-shifted when the phase changed from the solution to the film, the interaction between the polymer chains was enhanced due to the aggregation in the solid state. However, the UV spectrum of P2 and P3 tended to be blue-shifted when the phase changed from the solution to a film, indicating that the 2D π-stacking between the polymer chains decreases. Therefore, the implemented spacer increases the electron-donating characteristics, which enhances the effects of the delocalized π–π* transition.[30]

To confirm the effects of the thiophene spacer on the difference in the energy level, cyclic voltammograms of thin films for P1–P3 were obtained with 0.1 M tetrabutylammonium hexafluorophosphate (TBAHFP) in an acetonitrile solution. The measurement results are shown in Fig. 3 and summarized in Table 2. The oxidation onset potentials (E^{ox}_{onset}) of P1, P2, and P3 were +1.52, +1.35, and +1.23 V, respectively, and their calculated HOMO levels were −5.89, −5.72, and −5.60 eV, respectively. Because the air oxidation threshold was −5.27 eV, the HOMO level should be less than this value to ensure the oxidation stability of the materials.[31]

By increasing the amount of thiophene implemented in the spacer, the HOMO energy level of the polymers tended to increase from 5.89 to −5.60 eV because the increased thiophene spacers led to an increase in the electron-donating properties. These results are consistent with those reported by You's group that the HOMO level of the polymers in the push–pull system is primarily determined by the donor strength[32] and with those reported by Lidzey *et al.* that the HOMO level increased due to the electron-donating properties of the thiophene spacer.[25,33] In our previous study, the photovoltaic properties were investigated by synthesizing a D–π-A polymer series, such as poly[alkylidenefluorene-*alt*-di-2-thienyl-2,1,3-benzothiadiazole].[8] The results of this study indicated that when the octoxy side chain was applied in benzothiadiazole, which served as an acceptor, the difference in the HOMO level of the polymers was insignificant. In addition, when an alkyl side chain was employed in the spacer, the HOMO level was deep, and the difference in the HOMO level was between 0.04 and 0.15 eV. However, in this paper, the HOMO level of the polymers increased by +0.29 eV due to an increase in the number of spacers, which confirmed that the HOMO level of the polymers was affected more by the number of spacers (the strength of donating properties of main chains of polymers) than by side-chain effects.

The LUMO levels calculated based on the differences in the HOMO energy levels and optical band gap energies of P1, P2, and P3 were −4.37 eV, −4.01 and −3.96 eV, respectively. The LUMO energy levels of the P2 and P3 polymers are within a reasonable range because the LUMO energy levels are far greater than those of $PC_{70}BM$ (approximately −4.3 eV). But P1 showed deeper LUMO energy levels compared to PCBM and the energy difference (ΔE) between the LUMO of the donor and the LUMO of the acceptor was only 0.07 eV. The J_{SC} of PSC with P1 : $PC_{70}BM$ suggests poor charge generation.

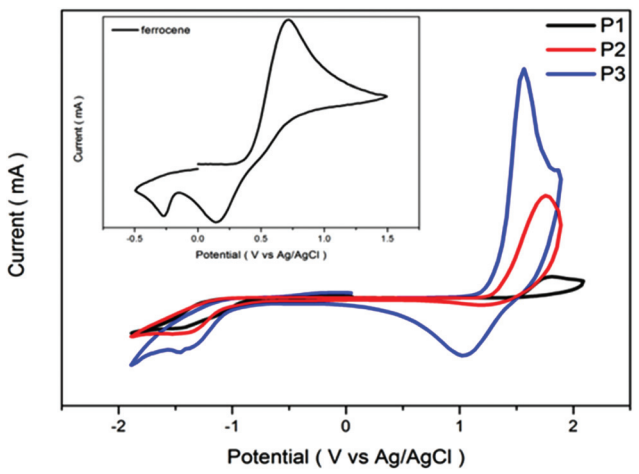

Fig. 3 Cyclic voltammograms of polymers.

2.3 Computational study of polymers

Simulations using density functional theory (DFT) were conducted to identify the electrical properties, molecular geometries, and electron density of the state distribution of the synthesized polymers. The DFT calculations were performed using Gaussian 09 with the hybrid B3LYP correlation functional and split valence 6-31G(d) basis set. Oligomers with two repeating units were selected for the calculation. The calculated HOMO and LUMO orbitals are shown in Fig. 4.

The HOMO orbitals are delocalized in the polymer main chain, and the LUMO orbitals are localized in the acceptor indigo dye due to the structural characteristics of the quinoid formed between the non-bonding electron pairs of nitrogen and sulfur, which exhibit electron-withdrawing characteristics.[34] As measured using a cyclic voltammogram, the lowest HOMO level (−5.24 eV) was obtained for P1, and the highest HOMO level (−4.86 eV) was obtained for P3 due to an increase in the electron-donating properties of the thiophene spacer.

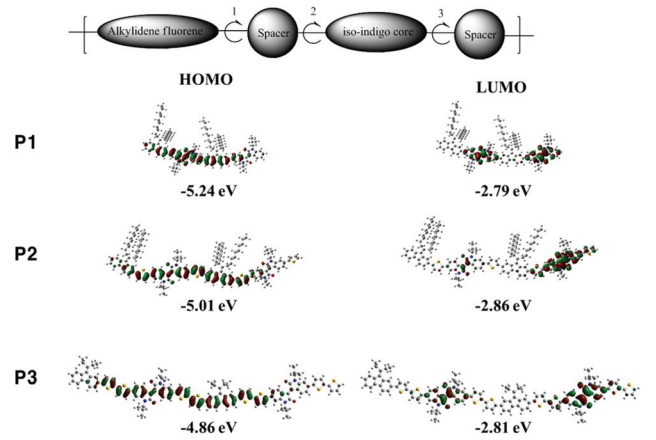

Fig. 4 Calculated LUMO and HOMO orbitals for the dimer models of the polymers.

Table 3 Calculated parameters

	Dihedral angle (°)				
Polymer	1	2	3	HOMO$^{cal.}$ [eV]	LUMO$^{cal.}$ [eV]
P1	35.5	—	—	−5.24	−2.79
P2	24.2	23.4	23.9	−5.01	−2.86
P3	25.9	20.8	19.6	−4.86	−2.81

The dihedral angles between the two spacer groups and the central isoindigo core and alkylidenefluorene were measured according to Fig. 4, and the results are summarized in Table 3. Based on these results, the internal steric hindrance of the polymers was observed according to the different lengths of the spacers. Dihedral angle 1 of P1 was 35.5° and dihedral angle 1 of P2 and P3 was 24.2° and 25.9°, respectively, which decreased by 10° or more compared to that in the absence of the spacer. Therefore, the steric hindrance of P1 was significantly greater than that of the other two polymers. In addition, dihedral angles 2 and 3 of P2 were 23.4° and 23.9°, respectively, and dihedral angles 2 and 3 of P3 were 20.8° and 19.6°, respectively. As the length of the spacer increased, the tilting angle of the polymers decreased because P3, which has a longer bithiophene spacer than P2, provides broader space in which the side chains can be released in the alkylidenefluorene and isoindigo core to ensure solubility of the polymers. The steric hindrance effectively decreases the π–π stacking between the polymers and the charge transport.[35]

Therefore, the implementation of a π linker reduces the steric hindrance between the alkylidenefluorene and the isoindigo core, the tilt angles decrease more as longer spacers are applied. Increased tilt angles break the conjugation reducing the current density during device manufacturing. Therefore, the current density of P3 will be the highest during the manufacture of OPV cells.

2.4 XRD measurement

To better understand the ordering characteristics of thin films and the π linker effect of the polymer, X-ray diffraction measurements were conducted at annealing temperatures. X-ray diffraction measurements of the polymer films, measured in the out-of-plane mode, were used to analyse the ordering structure in Fig. 5(a).

The thin film of P1 and P2 measured in the out-of-plane mode exhibited clear, sharp diffraction peaks at 4.32° and 4.52°, which indicates the formation of a (100) lamellar structure with high crystallinity. The results of calculation using Bragg's law ($\lambda = 2d\sin\theta$) indicated that the highly ordered (100) lamellar d-spacings (d_l) were 20.43 and 19.53 Å. However, unlike the other two polymers, P3 exhibited a small (100) peak at 4.76°, and the d_l calculated for this state was 18.54 Å. This is in good agreement with Erjun Zhou and Keisuke Tajima's work. Erjun Zhou *et al.* reported dithienopyrrole-based donor–acceptor type copolymers with various thienyl spacers. In the out-of-plane XRD measurement, the polymer which does not have a spacer showed a diffraction peak near 6°. But on increasing the number of spacers, the polymers did not show (100) diffraction peaks.[16] The broad diffraction peaks of the (010) crystal planes, which are related to the π–π stacking, were observed at 20.97°, 21.89°, and 24.48° for P1, P2, and P3, respectively. The π–π stacking distances (d_π) of P1, P2, and P3 were 4.2, 4.1, and 3.6 Å, respectively. The d_l- and d_π-spacing (*i.e.* the distances between the polymer chains of the P1–P3 polymers) decreased when going from P1 to P3. This result is in agreement with the DFT results where the tilt angle decreased as the spacer became longer, alleviating the steric hindrance between the alkylidenefluorene and the isoindigo core.

XRD measurements were conducted to validate the structural arrangement of the PCBM and polymer blended films (Fig. 5(b)). Strong (010) diffraction peaks due to the crystallinity of fullerene were measured at 18.81°, 18.61°, and 18.53° in the out-of-plane measurements of the polymer : $PC_{70}BM$ blend films. The interlamellar spacings of the P1–P3 : $PC_{70}BM$ thin films calculated using the 2θ value of the (010) peaks were 4.72, 4.77, and 4.79 Å, respectively. These values increase by 0.52, 0.67, and 1.12 Å, respectively, compared with the d_π value measured in the polymer thin film. This result means that $PC_{70}BM$ has penetrated deeply between the polymer chains.[36] However, $PC_{70}BM$ did not penetrate the intermolecular structure of P1 and P2, and they exist separately. In addition, the intensity of the (100) peak decreased for the diffraction peak of the P1 and P2 polymer thin films, confirming that blending with $PC_{70}BM$ interrupted the molecular arrangement of P1 and P2. However, a higher order of the lamellar scattering was observed in the P3 : $PC_{70}BM$ blend film, because the intensity of the (100) peak, which was recorded to be very low when only the P3 polymer was measured, increased when $PC_{70}BM$ was added.

Fig. 3(c) and (d) present the XRD profiles of the polymer and polymer : PCBM blended thin films measured in the

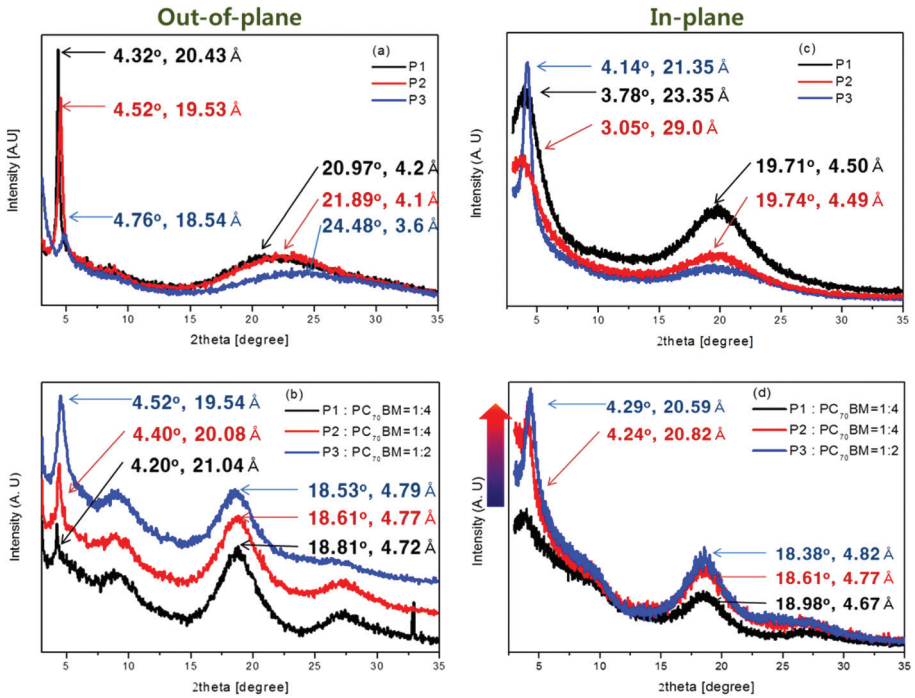

Fig. 5 X-ray diffraction pattern of polymers on a silicon wafer and a polymer : $PC_{70}BM$ blend on silicon wafer out-of-plane mode (a, b) and in-plane mode (c, d).

in-plane mode, respectively. The XRD profiles for P3 in the in-plane mode had one diffraction peak at a low (2θ = 4.14°) angle, which suggests that the P3 thin films formed a face-on structure. In contrast, the thin film of P1 and P2 showed XRD peaks at both low and high angles in the in-plane mode, demonstrating that this crystal structure had a mixed bimodal orientation. In Fig. 3(d), all of polymer : PCBM blend films showed XRD peaks at both low and high angles in the in-plane mode. The P3 : PCBM blended thin film showed the strongest diffraction peak at 4.29° in the in-plane mode. But low angle diffraction peaks tended to decrease in the in-plane mode XRD profile with the decreasing number of spacers. It means that the predominant crystalline structure within polymer : $PC_{70}BM$ blend films was changed from edge-on to face-on when the number of spacers was increased.

2.5 Photovoltaic properties

To determine the photovoltaic (PV) properties as a function of the spacer, BHJ PSCs were fabricated. Fig. 6(a) shows the *J–V* curves of the BHJ PCSs, and Fig. 6(b) shows the incident photon to charge carrier efficiency (IPCE). The PV properties of the three polymers were evaluated by manufacturing PSC devices with ITO/PEDOT : PSS/polymer : $PC_{70}BM/BaF_2$/Ba/Al structures. All of the fabricated devices were encapsulated in a glove box. The *J–V* characteristics were measured under an ambient atmosphere with an active area of 4 mm^2, and their performances were measured under 100 mW cm^{-2} AM 1.5 G illumination. The ratio of the polymer to $PC_{70}BM$ was adjusted from 1 : 1 to 1 : 4 (by weight) and the optimized conditions were 1 : 4 (P1, P2) and 1 : 2 (P3). The polymer active layers were spin-coated from solutions in σ-dichlorobenzene (ODCB). Table 4 and Table S2† summarize the photovoltaic response data including V_{OC}, J_{SC}, FF, and PCEs. OPV current density–voltage (*J–V*) plots, under standard illumination, for the solar cells based on P1–P3 : $PC_{70}BM$ active blends are shown in Fig. 6.

In P1, the open circuit voltage (V_{OC}) was 1.0 V, the short-circuit current density (J_{SC}) was 0.07 mA cm^2, and the FF was 49.1% to yield a PCE of 0.04%. In P2, a PCE of 0.66% was observed at a V_{OC} of 0.858 V, a J_{SC} of 1.4 mA cm^{-2}, and an FF of 54.2%, and P3 exhibited a PCE of 3.0% at a V_{OC} of 0.798 V, a J_{SC} of 7.3 mA cm^{-2}, and a FF of 51.6%. Because the exciton dissociation rate was low due to the low extinction coefficient, wide band gap, and excessive steric hindrance, low J_{SC} values were recorded resulting in a low PCE for P1. When the spacer was used, the band gap decreased, and the extinction coefficient increased due to the increase in conjugation length and planarity, which caused an increase in J_{SC} and device performance values. When $PC_{70}BM$ was blended with P1–P3, the regularity of the molecular arrangement of P1 and P2 decreased while P3 formed a higher-order lamellar structure.[37] This result is in good agreement with the increase in crystallinity where the active layer of P3 : $PC_{70}BM$ exhibits a rich face-on structure, as shown in the XRD measurement in Fig. 5. However, the V_{OC} decreases. The V_{OC} values of the devices created from the polymer : $PC_{70}BM$ (*i.e.*, blending the P1–P3 polymers) were recorded to be 1.0, 0.858 and 0.798 V, respectively. The V_{OC} is determined according to the difference

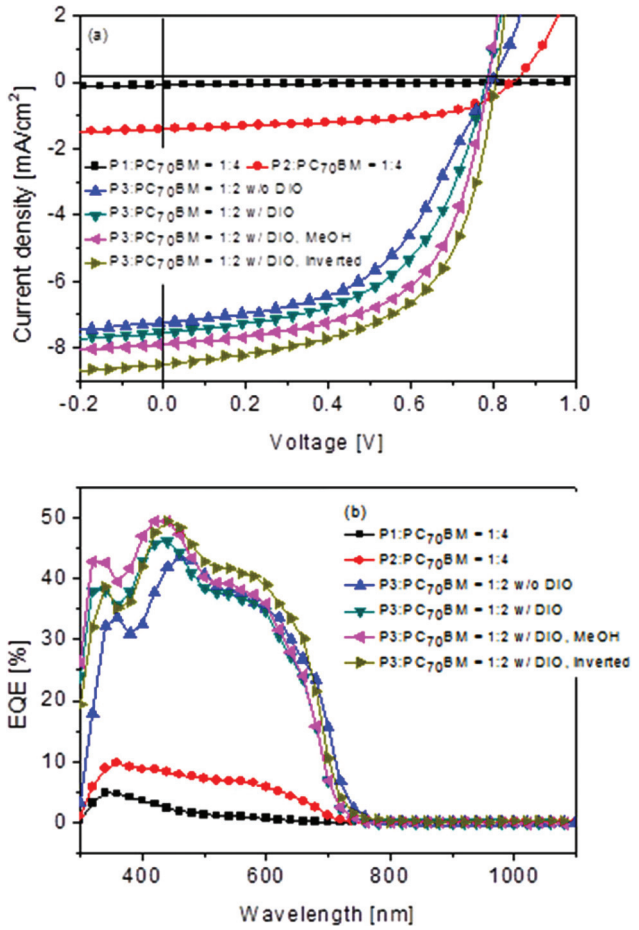

Fig. 6 J–V curves of the PSC based on polymer : $PC_{70}BM$ (a) under the illumination of AM 1.5G, 100 mW cm^{-2}. The IPCE spectra of the PSC based on polymer : $PC_{70}BM$ (b).

between the HOMO energy level in the polymers and the LUMO energy levels in PCBM. P1 exhibited the highest V_{OC} because it has a deeper-lying HOMO level. The electron-donating characteristics were reinforced in P2 and P3 with the implementation of the spacers, leading to increases in the HOMO level with a reduction in the V_{OC} values.

These devices exhibited adequately wide EQE graphs in the visible region (300–700 nm) and large EQE values in the absorbance range of 300–750 nm but lower values above 750 nm.

The P3 : $PC_{70}BM$ blend-based devices exhibited the highest EQE (up to 43.5%) at 460 nm, which is in agreement with the result for the highest photocurrent value. P1 and P2 showed 4.85% and 9.77% EQE, respectively.

Therefore, changes in the energy level of the polymers and steric hindrance are dependent on the implementation of a spacer and its length.

P3, which has the highest HOMO level due to bithiophene, exhibited the lowest V_{OC}. But the small steric hindrance contributed to the increasing J_{SC} greatly by the approach of the PCBM resulting in an increase in the crystallinity.

To optimize and enhance the performance of the P3 device, 3 vol% 1,8-diiodooctane (DIO) was added as the solvent additive. It leads to a significant 10% enhancement in PCE with a simultaneous improvement in J_{SC} (7.3–7.5 mA cm^{-2}) and FF (51.6–55.2%). Recently post-deposition methanol treatment has proven to be an effective method to obtain nanoscale morphology for the active layer by controlling the phase separation between the donor and the acceptor. Methanol has been widely used in surface engineering by incorporation of an interlayer in BHJ PSCs.[38] As shown in Fig. 6(a), after treating the active layer with methanol, the PCE increased from 3.3 to 3.6% for the P3 device. It showed a slightly increased J_{SC} from 7.5 to 7.7 mA cm^{-2} and a FF from 55.2 to 57.6%. The $PC_{70}BM$ molecules may migrate upside more easily between the polymer chains by methanol treatment, which then effectively increases the interfacial area between the polymers and the $PC_{70}BM$ molecules with maintaining nanoscopically connected each domain. This is supported by the results of the morphology studies (Fig. 7).

Compared with conventional OPVs, inverted type devices can also take advantage of the vertical phase separation and concentration gradient in the active layer, which is naturally self-encapsulated because air-stable metals are used as the top electrode.[39] So we manufactured inverted PSC devices with ITO/ZnO/P3 : $PC_{70}BM/MoO_3$/Ag structures, and PCE was increased to 4.0%. It showed a J_{SC} = 8.2 mA cm^{-2} and a FF = 58.7%.

2.6 Morphology analysis and charge carrier mobility

The hole mobility of the polymer is very important for the photovoltaic performance of BHJ solar cells. We used a space charge limited current (SCLC) model, which is based on the Poole–Frenkel law, to determine the hole mobility in blends

Table 4 Photovoltaic properties of polymers

Polymer	Device structure	Solvent + additive	Solvent treatment	$PC_{70}BM$ ratios	V_{OC} [V]	J_{SC} [mA cm^{-2}]	FF [%]	PCE [%]
P1	Conventional	ODCB + none	None	1 : 4	1.0	0.07 ± 0.003	49.1 ± 1.4	0.04 ± 0.006
P2	Conventional	ODCB + none	None	1 : 4	0.858 ± 0.02	1.4 ± 0.2	54.2 ± 1.4	0.66 ± 0.04
P3	Conventional	ODCB + none	None	1 : 2	0.798 ± 0.02	7.3 ± 0.3	51.6 ± 0.9	3.00 ± 0.1
P3	Conventional	CB + DIO	None	1 : 2	0.778 ± 0.02	7.5 ± 0.2	55.2 ± 2.0	3.3 ± 0.1
	Conventional	CB + DIO	MeOH		0.778 ± 0.02	7.7 ± 0.2	57.6 ± 0.2	3.6 ± 0.2
	Inverted	CB + DIO	None		0.798	8.2 ± 0.3	58.7 ± 0.7	4.0 ± 0.2

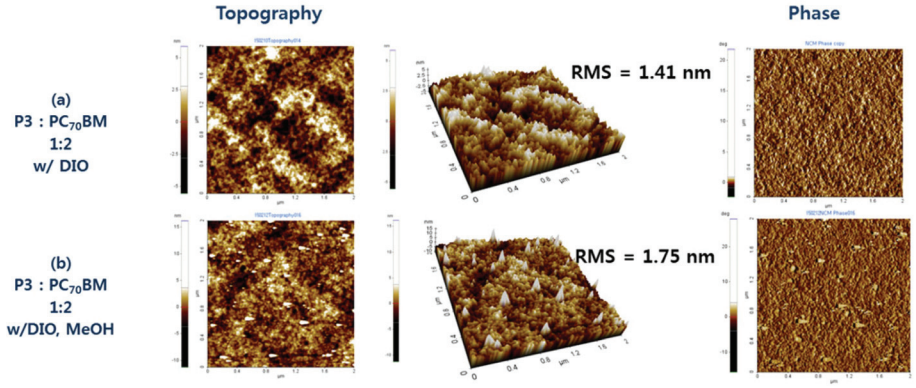

Fig. 7 Topographic AFM images of polymer : $PC_{70}BM$ (a) P3 : $PC_{70}BM$ 1 : 2 w/w with DIO (2 × 2 μm^2), (b) P3 : $PC_{70}BM$ 1 : 2 w/w with DIO + MeOH treatment (2 × 2 μm^2).

containing the polymer and $PC_{70}BM$. The result can be obtained by plotting $\ln(JL^3/V^2)$ *vs.* $(V/L)^{1/2}$ and is shown in ESI.† Herein, J refers to the current density, d refers to the thickness of the device, and $V = V_{appl} - V_{bi}$, where V_{appl} is the applied potential and V_{bi} is the built-in potential. Hole-only devices were fabricated with a diode configuration of ITO (170 nm)/PEDOT : PSS (40 nm)/polymer : $PC_{70}BM$/MoO_3 (30 nm)/Al (100 nm).

According to Fig. S2–S4† for $\ln(JL^3/V^2)$ *vs.* $(V/L)^{1/2}$ and the equation, the hole mobilities of the three blended polymers are 5.76×10^{-5}, 4.61×10^{-4}, and 1.97×10^{-3} $cm^2\ V^{-1}\ s^{-1}$.

The P3 : PCBM blend exhibited the highest mobility due to the high crystalline morphology of the blend film and the larger planar structure of the polymer.

The surface morphology of the polymer blend is another critical factor that determines the efficiency of PSCs. Therefore, the morphologies of the polymer : PCBM blend films were characterized using atomic force microscopy (AFM) and are shown in Fig. S7.†

The dark-colored and light-colored areas correspond to the PCBM domains and polymers, respectively. The surfaces of the P3 : $PC_{70}BM$ blended films were smooth with nanoscale features. The good intermixing between the polymer and $PC_{70}BM$ resulted in the optimal formation of channels in the polymers. This result is in agreement with the high J_{SC} in P3. However, the black dots due to the high aggregation of the PCBM domain were observed in the P1 and P2 blend films. A significant phase separation was observed, especially in P1, which had the roughest surface with a root-mean-square (RMS) roughness of 7 nm. This is due to the difficulty PCBM experiences approaching the polymer chain due to significant steric hindrance. When a long π-linker was implemented in the polymer backbone for P1–P3, the RMS roughness tended to decrease, and J_{SC} increased.

We also directly examined the surface morphology with and without methanol exposure *via* AFM. The AFM topography images are shown in Fig. 7.

In the case of P3 : $PC_{70}BM$ blends, it could be observed that the blend film without solvent exposure exhibited relatively clear phase separation between the polymer and $PC_{70}BM$ with relatively large (100 − 500 nm) $PC_{70}BM$ globular clusters that may originate during the drying of the film. In contrast, after solvent treatment, the surface of the blend film demonstrated a more uniform distribution of P3 and $PC_{70}BM$, and the formation of interpenetrating morphologies at the small scale of 100 − 200 nm $PC_{70}BM$ clusters for the methanol-treated device. This relatively smooth surface and more fine structure are beneficial to the charge transportation, thus leading to an increase in J_{SC} and the device efficiency.

3. Experimental

3.1 Materials

All starting materials were purchased from Sigma Aldrich and Alfar Aesar and used without further purification. Toluene and tetrahydrofuran (THF) were distilled from benzophenone ketyl and sodium. The following compounds were synthesized by following modified literature procedures: 2,7-bis(4,4,5,5-tetramethyl-1,3,2-dioxaborolan-2-yl)-9-(1-decylundecylidene)fluorene (AF),[27,40] 6,6′-dibromo-*N*,*N*′-(2-octyldodecyl)isoindigo (A0),[41] and 2T.[42]

3.2 Polymerization

3.2.1 Poly[2,7-bis-9-(1-decylundecylidene)fluorene-*alt*-*N*,*N*′-(2-octyldodecyl)-6,6′-isoindigo] (P1). Reddish black solid, 0.285 g (yield = 76%). ^{1}H NMR (400 MHz, $CDCl_3$, d): 9.30–9.25 (m, 2H), 8.08 (s, 2H), 7.91–7.89 (m, 2H), 7.45 (m, 2H), 7.37–7.34 (m, 2H), 7.08 (m, 2H), 3.77 (m, 4H), 2.91 (m, 3H), 2.00–1.82 (d, 2H), 1.40–1.21 (m, 92H), 0.83 (s, 18H).

3.2.2 Poly[2,7-bis-9-(1-decylundecylidene)fluorene-*alt*-*N*,*N*′-(2-octyldodecyl)-6,6′-dithiphen-2-yl-isoindigo] (P2). Blue black solid, 0.29 g (yield = 67%). ^{1}H NMR (400 MHz, $CDCl_3$, d): 9.15–8.95 (m, 2H), 8.10–6.80 (m, 12H), 6.70–6.50 (m, 2H), 3.80–3.60 (m, 4H), 2.95–2.65 (m, 4H), 2.00–0.95 (m, 98H), 0.95–0.65 (s, 16H).

3.2.3 Poly[2,7-bis-9-(1-decylundecylidene)fluorene-*alt*-*N*,*N*′-(2-octyldodecyl)-6,6′-di-2,2′-bithiphen-5-yl-isoindigo] (P3).

Greenish black solid, 0.14 g (yield = 27%). ^{1}H NMR (400 MHz, $CDCl_3$, d): 9.15–8.95 (m, 2H), 8.10–6.80 (m, 14H), 6.70–6.50 (m, 2H), 3.80–3.60 (m, 4H), 2.95–2.65 (m, 3H), 2.00–0.95 (m, 98H), 0.95–0.65 (s, 16H).

3.3 Measurements

The ^{1}H-NMR (400 MHz) spectra were recorded using a Brüker AMX400 spectrometer in $CDCl_3$, and the chemical shifts were recorded in units of ppm with TMS as the internal standard. The absorption spectra were recorded using an Agilent 8453 UV-visible spectroscopy system. The solutions that were used for the UV-visible spectroscopy measurements were dissolved in chloroform at a concentration of 10 μg ml^{-1}. The films were drop-coated from the chloroform solution onto a quartz substrate. All of the GPC analyses were carried out using THF as the eluent and a polystyrene standard as the reference. The TGA measurements were performed using a TG 209 F3 thermogravimetric analyzer. The cyclic voltammetric waves were produced using a Zahner IM6eX electrochemical workstation with a 0.1 M acetonitrile (substituted with nitrogen for 20 min) solution containing tetrabutylammonium hexafluorophosphate (Bu_4NPF_6) as the electrolyte at a constant scan rate of 50 mV s^{-1}. ITO, a Pt wire, and silver/silver chloride [Ag in 0.1 M KCl] were used as the working, counter, and reference electrodes, respectively. The electrochemical potential was calibrated against Fc/Fc^+. The HOMO levels of the polymers were determined using the oxidation onset value. Onset potentials are values obtained from the intersection of the two tangents drawn at the rising current and the baseline changing current of the CV curves. The LUMO levels were calculated from the differences between the HOMO energy levels and the optical band-gaps, which were determined using the UV-Vis absorption onset values in the films. The current density–voltage (J–V) curves of the photovoltaic devices were measured using a computer-controlled Keithley 2400 source measurement unit (SMU) that was equipped with a Class A Oriel Solar Simulator under illumination of AM 1.5G (100 mW cm^{-2}). Topographic images of the active layers were obtained through atomic force microscopy (AFM) in tapping mode under ambient conditions using an XE-100 instrument.

3.4 Photovoltaic cell fabrication and treatment

All the bulk-heterojunction PV cells were prepared using the following device fabrication procedure. The glass/indium tin oxide (ITO) substrates [Sanyo, Japan (10 Ω γ^{-1})] were sequentially patterned lithographically, cleaned with a detergent, ultrasonicated in deionized water, acetone, and isopropyl alcohol, dried on a hot plate at 120 °C for 10 min, and treated with oxygen plasma for 10 min to improve the contact angle just before film coating. Poly(3,4-ethylene-dioxythiophene) : poly(styrene-sulfonate) (PEDOT : PSS, Baytron P 4083 Bayer AG) was passed through a 0.45 mm filter before being deposited on ITO at a thickness of *ca.* 32 nm by spin-coating at 4000 rpm in air, and then dried at 120 °C for 20 min inside a glove box. A blend of 1-(3-methoxycarbonyl)propyl-1-phenyl-[6,6]-C71 ($PC_{70}BM$) and the polymer [1 : 1 (w/w), 1 : 4 (w/w)] at a concentration of 7.5 mg mL^{-1} in chlorobenzene was stirred overnight, filtered through a 0.2 mm poly(tetrafluoroethylene) (PTFE) filter, and then spin-coated (500–3000 rpm, 30 s) on top of the PEDOT : PSS layer. The device was completed by depositing thin layers of BaF_2 (1 nm) and Ba (2 nm) as an electron injection cathode, followed by the deposition of a 200 nm thick aluminum layer at a pressure less than 10^{-6} torr. The active area of the device was 4 mm^2. Finally, the cell was encapsulated using UV-curing glue (Nagase, Japan).

The hole-only devices were fabricated with a diode configuration of ITO (170 nm)/PEDOT : PSS (40 nm)/Polymer : $PC_{70}BM$/MoO_3 (30 nm)/Al (100 nm). The hole mobility of the active layers was calculated from the SCLC using the J–V curves of the hole-only devices in the dark as follows:

$$J = \frac{9}{8}\varepsilon_r\varepsilon_0\mu_{h(e)}\frac{V^2}{L^3}\exp\left(0.89\sqrt{\frac{V}{E_0L}}\right)$$

where ε_0 is the permittivity of free space (8.85×10^{-14} F cm^{-1}), ε is the dielectric constant (assumed to be 3, which is a typical value for conjugated polymers) of the polymer, μ is the zero-field mobility of holes (electrons), L is the film thickness, and $V = V_{appl} - V_r + V_{bi}$, where V_{appl} is the applied voltage to the device, V_r is the voltage drop due to the series resistance across the electrodes, and V_{bi} is the built-in voltage.

4. Conclusions

In this study, we successfully synthesized three polymers (*i.e.* P1, P2, and P3) with alkylidene fluorene as the donor and isoindigo derivatives as acceptors using the Suzuki coupling reaction by adjusting the thiophene spacer length. As the number of thiophene spacers increased, the band gap of polymers decreased and the HOMO level tended to increase. Although P1 and P2 exhibited edge-on rich orientation in the XRD measurements, when the polymers were blended with $PC_{70}BM$, P1 and P2 only exhibited a peak due to the crystallinity of $PC_{70}BM$ and a substantial decrease in the (100) peak of the polymer. P3 allowed for easier access of $PC_{70}BM$, and an increased face-on crystallinity peak was observed in in-plane mode of XRD measurements. Although V_{OC} decreased due to the increase in the HOMO level resulting from the implementation of the bithiophene spacer, the best performance was observed when PCE = 4.2% in the P3 : $PC_{70}BM$ structure (1 : 2, w/w).

Acknowledgements

This research was supported by the National Research Foundation of Korea Grant funded by the Korean Government (MEST) (NRF-2012M1A2A2671703) and by the New & Renewable Energy Core Technology Program of the Korea Institute of Energy Technology Evaluation and Planning (KETEP) grant funded by the Ministry of Trade, industry & Energy (MI, Korea) (no. 20133030000180).

Notes and references

1 K. W. Song, M. H. Choi, H. J. Song, S. W. Heo, J. Y. Lee and D. K. Moon, *Sol. Energy Mater. Sol. Cells*, 2014, **120**(Part A), 303–309.
2 M. H. Choi, K. W. Song, S. W. Heo, Y. W. Han and D. K. Moon, *J. Ind. Eng. Chem.*, DOI: 10.1016/j.jiec.2014.10.045.
3 Z. He, C. Zhong, X. Huang, W.-Y. Wong, H. Wu, L. Chen, S. Su and Y. Cao, *Adv. Mater.*, 2011, **23**, 4636–4643.
4 C. Cabanetos, A. El Labban, J. A. Bartelt, J. D. Douglas, W. R. Mateker, J. M. J. Fréchet, M. D. McGehee and P. M. Beaujuge, *J. Am. Chem. Soc.*, 2013, **135**, 4656–4659.
5 M. A. Green, K. Emery, Y. Hishikawa, W. Warta and E. D. Dunlop, *Prog. Photovoltaics Res. Appl.*, 2013, **21**, 1–11.
6 H. J. Song, D. H. Kim, E. J. Lee, J. R. Haw and D. K. Moon, *Sol. Energy Mater. Sol. Cells*, 2014, **123**, 112–121.
7 A. T. Yiu, P. M. Beaujuge, O. P. Lee, C. H. Woo, M. F. Toney and J. M. J. Fréchet, *J. Am. Chem. Soc.*, 2011, **134**, 2180–2185.
8 K. W. Song, H. J. Song, T. H. Lee, S. W. Heo and D. K. Moon, *Polym. Chem.*, 2013, **4**, 3225–3235.
9 M. S. Chen, J. R. Niskala, D. A. Unruh, C. K. Chu, O. P. Lee and J. M. J. Fréchet, *Chem. Mater.*, 2013, **25**, 4088–4096.
10 A. Salleo, R. J. Kline, D. M. DeLongchamp and M. L. Chabinyc, *Adv. Mater.*, 2010, **22**, 3812–3838.
11 J. Liu, H. Choi, J. Y. Kim, C. Bailey, M. Durstock and L. Dai, *Adv. Mater.*, 2012, **24**, 538–542.
12 M. Heeney, C. Bailey, M. Giles, M. Shkunov, D. Sparrowe, S. Tierney, W. Zhang and I. McCulloch, *Macromolecules*, 2004, **37**, 5250–5256.
13 V. Coropceanu, J. Cornil, D. A. da Silva Filho, Y. Olivier, R. Silbey and J.-L. Brédas, *Chem. Rev.*, 2007, **107**, 926–952.
14 M. R. Hammond, R. J. Kline, A. A. Herzing, L. J. Richter, D. S. Germack, H.-W. Ro, C. L. Soles, D. A. Fischer, T. Xu, L. Yu, M. F. Toney and D. M. DeLongchamp, *ACS Nano*, 2011, **5**, 8248–8257.
15 J. Eggert Carlé, J. Wenzel Andreasen, M. Jørgensen and F. Christian Krebs, *Sol. Energy Mater. Sol. Cells*, 2010, **94**, 774–780.
16 Y. Geng, J. Cong, K. Tajima, Q. Zeng and E. Zhou, *Polym. Chem.*, 2014, **5**, 6797–6803.
17 J. Mei, K. R. Graham, R. Stalder and J. R. Reynolds, *Org. Lett.*, 2010, **12**, 660–663.
18 R. Stalder, J. Mei and J. R. Reynolds, *Macromolecules*, 2010, **43**, 8348–8352.
19 X. Xu, P. Cai, Y. Lu, N. S. Choon, J. Chen, X. Hu and B. S. Ong, *J. Polym. Sci., Part A: Polym. Chem.*, 2013, **51**, 424–434.
20 D. H. Kim, A. L. Ayzner, A. L. Appleton, K. Schmidt, J. Mei, M. F. Toney and Z. Bao, *Chem. Mater.*, 2012, **25**, 431–440.
21 T. Lei, J.-H. Dou, Z.-J. Ma, C.-J. Liu, J.-Y. Wang and J. Pei, *Chem. Sci.*, 2013, **4**, 2447–2452.
22 Y. K. Voronina, D. B. Krivolapov, A. V. Bogdanov, V. F. Mironov and I. A. Litvinov, *J. Struct. Chem.*, 2012, **53**, 413–416.
23 Z. Peng, W. Si, S. Lin, H. Miao, H. Fu, M. Xie, H. Ma, H. Zeng and Z. Su, *Eur. Polym. J.*, 2002, **38**, 1635–1643.
24 Z. G. Zhang and J. Wang, *J. Mater. Chem.*, 2012, **22**, 4178–4187.
25 M. S. Almeataq, H. Yi, S. Al-Faifi, A. A. B. Alghamdi, A. Iraqi, N. W. Scarratt, T. Wang and D. G. Lidzey, *Chem. Commun.*, 2013, **49**, 2252–2254.
26 C. L. Chochos and S. A. Choulis, *Prog. Polym. Sci.*, 2011, **36**, 1326–1414.
27 M. Heeney, C. Bailey, M. Giles, M. Shkunov, D. Sparrowe, S. Tierney, W. Zhang and I. McCulloch, *Macromolecules*, 2004, **37**, 5250–5256.
28 R. Stalder, J. Mei, J. Subbiah, C. Grand, L. A. Estrada, F. So and J. R. Reynolds, *Macromolecules*, 2011, **44**, 6303–6310.
29 T. Yasuda, T. Imase and T. Yamamoto, *Macromolecules*, 2005, **38**, 7378–7385.
30 L. Dong, Y.-C. Chiu, C.-C. Chueh, A.-D. Yu and W.-C. Chen, *Polym. Chem.*, 2014, **5**, 6834–6846.
31 D. M. de Leeuw, M. M. J. Simenon, A. R. Brown and R. E. F. Einerhand, *Synth. Met.*, 1997, **87**, 53–59.
32 H. Zhou, L. Yang and W. You, *Macromolecules*, 2012, **45**, 607–632.
33 H. Yi, S. Al-Faifi, A. Iraqi, D. C. Watters, J. Kingsley and D. G. Lidzey, *J. Mater. Chem.*, 2011, **21**, 13649–13656.
34 Z. Ma, E. Wang, M. E. Jarvid, P. Henriksson, O. Inganas, F. Zhang and M. R. Andersson, *J. Mater. Chem.*, 2012, **22**, 2306–2314.
35 H. Zhou, L. Yang, S. Xiao, S. Liu and W. You, *Macromolecules*, 2010, **43**, 811–820.
36 W. Lee, G.-H. Kim, S.-J. Ko, S. Yum, S. Hwang, S. Cho, Y.-H. Shin, J. Y. Kim and H. Y. Woo, *Macromolecules*, 2014, **47**, 1604–1612.
37 N. C. Cates, R. Gysel, Z. Beiley, C. E. Miller, M. F. Toney, M. Heeney, I. McCulloch and M. D. McGehee, *Nano Lett.*, 2009, **9**, 4153–4157.
38 K. Kranthiraja, K. Gunasekar, W. Cho, M. Song, Y. G. Park, J. Y. Lee, Y. Shin, I.-N. Kang, A. Kim, H. Kim, B. Kim and S.-H. Jin, *Macromolecules*, 2014, **47**, 7060–7069.
39 S. Kim, J. H. Koh, X. Yang, W. S. Chi, C. Park, J. W. Leem, B. Kim, S. Seo, Y. Kim, J. S. Yu, J. H. Kim and E. Kim, *Adv. Energy Mater.*, 2014, **4**, 1301338.
40 J.-Y. Lee, W.-S. Shin, J.-R. Haw and D.-K. Moon, *J. Mater. Chem.*, 2009, **19**, 4938–4945.
41 H. Bronstein, Z. Chen, R. S. Ashraf, W. Zhang, J. Du, J. R. Durrant, P. Shakya Tuladhar, K. Song, S. E. Watkins, Y. Geerts, M. M. Wienk, R. A. J. Janssen, T. Anthopoulos, H. Sirringhaus, M. Heeney and I. McCulloch, *J. Am. Chem. Soc.*, 2011, **133**, 3272–3275.
42 K. Parab, K. Venkatasubbaiah and F. Jäkle, *J. Am. Chem. Soc.*, 2006, **128**, 12879–12885.